International Journal of Biological Macromolecules 332 (2025) 148727

Contents lists available at ScienceDirect

International Journal of Biological Macromolecules

journal homepage: www.elsevier.com/locate/ijbiomac

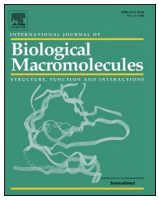

Lipase-mediated bi-phasic modification of citrus pectin (MCP) and expedition of its packaging film characteristics

Chandra Mohan Chandrasekar [a,b,*], Daniele Carullo [a], Francesca Saitta [a], Tommaso Bellesia [a], Enrico Caneva [c], Carlo Baschieri [c], Marco Signorelli [a], Alberto Giuseppe Barbiroli [a], Dimitrios Fessas [a], Stefano Farris [a], Diego Romano [a,*]

[a] Department of Food Environmental and Nutritional Sciences (DeFENS), University of Milan (UNIMI), Milan, Italy
[b] USDA - ARS, US Horticultural Research Laboratory, Citrus & Other Subtropical Products Research Unit, 2001 South Rock Road, Fort Pierce, FL, 34945, USA
[c] UNITECH COSPECT: Comprehensive Substances characterisation via advanced sPECTtrometry, Milan, Italy

A B S T R A C T

This study focuses on the enzymatic modification of citrus pectin (CP) with stearic acid (SA) in a bi-phasic reaction system, with the aim of enhancing its application in packaging films. We employed a central composite design of experiments and principal component analysis to investigate the effects of pH, reaction temperature, and time on the modification process. The principal component analysis identified reaction time and temperature as critical factors influencing modification, leading to a maximum modification percentage of 43.35 ± 1.81 % at pH 7, 60 °C, and 72 h. The physical characteristics of modified citrus pectin (MCP) showed increased molecular weight and particle size, thereby influencing the packaging films' mechanical and barrier properties. Zeta potential measurements indicated improved dispersion stability, resulting in homogeneous film formation. Chemical analyses confirmed the structural modifications in MCP. The characterisation of MCP-based films revealed a trade-off between properties: a significant reduction in mechanical strength was observed, offset by substantial improvements in water and oxygen barrier performance. This work positions MCP as a functional biopolymer for developing advanced composite packaging materials with tailored barrier properties.

Abbreviations

CP	Citrus Pectin
MCP	Modified Citrus Pectin
FTIR	Fourier transform infrared spectroscopy
TGA	Thermogravimetric analysis
DSC	Differential scanning calorimetry
NMR	Nuclear magnetic resonance
COSY	Correlated spectroscopy
HSQC	Heteronuclear Single Quantum Coherence
HMBC	Heteronuclear Multiple Bond Correlation
CA	Contact angle
OTR	Oxygen transmission rate
WVTR	Water vapour transmission rate
SEM	Scanning electron microscopy
AFM	Atomic force microscopy

Keywords

Biopolymer modification
Pectin-graft-stearic acid
Lipase catalysis
Bi-phasic system
Barrier properties
Sustainable packaging

1. Introduction

Pectin, a natural polysaccharide in various fruits and vegetables, is a fundamental ingredient in many culinary and industrial applications [1]. Renowned for its remarkable gelling properties, pectin is pivotal in creating jams, jellies, and preserves, lending them their characteristic texture and consistency [2–4]. Beyond the realm of food, pectin finds extensive use in pharmaceuticals and cosmetics for its thickening and stabilising abilities. This versatile compound, with its diverse applications and widespread availability in nature, stands as a testament to the ingenuity of organic chemistry and the manifold ways in which we harness the natural world's resources [1,5]. In recent years, the development of pectin-based packaging systems has gained overwhelming attention from many researchers [6–10]. Pectin-based packaging films represent an innovative approach to sustainable and eco-friendly packaging solutions. Pectin offers a biodegradable and renewable alternative to traditional petroleum-based plastics [10]. These

* Corresponding authors at: Department of Food Environmental and Nutritional Sciences (DeFENS), University of Milan (UNIMI), Milan, Italy.
E-mail addresses: master.chandramohan@gmail.com, chandra.chandrasekar@unimi.it (C.M. Chandrasekar), Diego.Romano@unimi.it (D. Romano).

https://doi.org/10.1016/j.ijbiomac.2025.148727
Received 12 August 2025; Received in revised form 31 October 2025; Accepted 1 November 2025
Available online 3 November 2025

packaging films are gaining attention for their ability to create flexible, transparent, and biodegradable materials suitable for various packaging applications. Pectin, when processed into films, exhibits excellent barrier properties against moisture, oxygen, and grease, making it ideal for packaging perishable goods such as fruits, vegetables, and baked goods [6,7].

The main limitation of pectin-based packaging films is their low water resistance capacities, which has hindered their industrial-level application. The effective bulk modification of pectin with hydrophobic functional groups can provide a ground-breaking path in the field of pectin-based packaging systems [7,9]. Enzymatic modification of polysaccharides has gained significant traction among researchers due to its eco-friendly, green technological process. [11] investigated the enzymatic amidation of pectin to improve its gelling properties. [12] have tried to develop an active packaging material with enzymatic grafting of resorcinol and 4-hexylresorcinol with pectin. A significant challenge in grafting a hydrophobic molecule, such as stearic acid, onto a hydrophilic polymer, such as pectin, is the immiscibility of the reactants. To overcome this, our study introduces a bi-phasic (water/hexane) reaction system. This system allows the pectin to be dissolved in the aqueous phase and the stearic acid in the organic phase. The reaction is catalyzed by a lipase, an enzyme known to exhibit high catalytic activity at the interface between aqueous and organic media. This approach provides an ideal environment for the esterification reaction to occur efficiently. Lipase-catalyzed reactions in non-aqueous or biphasic systems are well documented for producing a variety of valuable esters and modified polymers and have been successfully applied to modify pectin with other functional molecules, sometimes exhibiting a dual role of hydrolysis and esterification. Even then, to the best of our knowledge, bulk enzymatic modification of pectin to improve its water-repelling capabilities has not yet been reported. With the basis mentioned above, we derived two hypotheses for our study: 1) Enzymatic bulk modification of pectin can be achieved in a bi-phasic reaction medium with lipase. 2) The bulk modification of pectin with stearic acid can improve the water-repelling capacity of the modified citrus pectin (MCP) based packaging films.

Thus, the main objective of this work is to modify citrus pectin with stearic acid using commercially available lipase in a biphasic reaction medium. Moreover, this study aims to develop MCP-based packaging films.

2. Materials and methods

2.1.1. Raw materials

Citrus pectin and nanocellulose were extracted from Citrus industrial wastes provided by the citrus fruit processing industry Ortogel SPA (Belpasso, Catania, Italy). The detailed extraction process and its characterisations were reported in our previous work [13]. All the analytical chemicals used in this study were purchased from Merck, Germany.

2.2. Modification of citrus pectin with stearic acid

3 g of citrus pectin was dissolved in 100 mL of distilled water in a magnetic stirrer operating at 600 rpm and 50 °C for 20 min. Then, 100 mL of hexane with an equal molar ratio of stearic acid was poured over the pectin solution and inoculated with 500 U of lipase (Lipase B from *Candida antarctica*, immobilized on macroporous acrylic resin, Novozym® 435, purchased from Sigma-Aldrich, St. Louis, MO, USA). This reaction mixture was made to operate under different pH conditions (6, 7, and 8) using phosphate buffer, different temperature conditions (40, 50, and 60 °C), and reaction time (24, 48, and 72 h), according to the central composite design of experiments constructed to study the effect of different operating conditions on the grafting of stearic acid with citrus pectin. The modification percentage of the pectin was semi-quantitatively estimated by the peak intensity ratio of approximately ~1735 cm^{-1} to that at around 1104 cm^{-1}. This ratiometric method, which normalizes the intensity of the new ester carbonyl peak (~1735 cm^{-1}) against the stable C-O-C glycosidic backbone peak (~1104 cm^{-1}), is a well-established technique for assessing the degree of modification and esterification in pectin and other polysaccharides, as mentioned by [11,12].

2.3. Characterisation of MCP

2.3.1. Particle size and ζ-potential

Both particle size and ζ-potential of the samples were measured by photon correlation spectroscopy experiments using dynamic light scattering (DLS) and electrophoretic light scattering (ELS) analyses, respectively, using a LitesizerTM 500 (Anton Paar, Rivoli, Italy) system at neutral pH [14]The tests were carried out at 25 °C, with a stabilisation time of 60 s, using the viscosity (0.8872 cP) and refractive index (1.33) of water as reference values. The software Kalliope (Anton Paar, Rivoli, Italy) used the non-negative least squares algorithm to retrieve the size distribution.

2.3.2. Thermogravimetric analysis and differential scanning calorimetry (TGA-DSC)

The thermal degradation properties of the extracted polysaccharides were analysed by thermogravimetric analysis (TGA) coupled with differential scanning calorimetry (DSC) [15]. A Setaram TG-DSC111 (Lyon, France) was used to simultaneously record the TG trace (mass versus temperature) and the thermal effects (heat flow versus temperature). A typical sample mass of about 15 mg was placed into an aluminium crucible and heated from 25 °C to 500 °C at a scanning rate of 2 °C/min under a nitrogen atmosphere. An empty aluminium crucible was used as a reference. Each run was repeated twice. All the TG traces reported in the figures were normalised to 100 mg of mass sample. Accordingly, the temperature derivative of the TG traces (DTG = dm(T)/dT) was expressed as mg•K^{-1}. Instead, all the DSC thermograms in the figures were normalised per mass of the initial sample, expressing the heat flow as W•g^{-1}.

2.3.3. Solid-state fourier transform infrared spectroscopy (FTIR)

FTIR analysis was performed using a Spectrum 100 instrument (Perkin Elmer Inc., Waltham, MA) coupled with an Attenuated Total Reflectance (ATR) accessory and a Ge/Ge crystal, fixed at an incident angle of 45°. All spectra were collected at a resolution of 4 cm^{-1} over a wavenumber range between 4000 cm^{-1} and 800 cm^{-1}, resulting from an average of 180 scans. A background scan of clean Ge crystal in the air was acquired before each scan [16].

2.3.4. Solid-state ^{13}C cross-polarization magic angle spinning (CP-MAS)

CP-MAS spectra were collected at 125.76 MHz on an Avance 500 MHz NMR Spectrometer (Bruker Italia s.r.l., Milan, Italy), operating at a magnetic field of 11.7 T and equipped with a 4 mm MAS probe, spinning the sample at the magic angle up to 15 kHz, which, with the addition of high power 1H decoupling capability, allows the decrease or the elimination of homo and heteronuclear anisotropies. All the samples were prepared by packing them in Zirconia (ZrO2) rotors, closed with Kel-F caps (50 μL internal volume), and the MAS rate was optimised to 10 kHz after running some experiments in the 2–15 kHz range. Cross polarization spectra, under Hartmann–Hahn conditions were recorded with a variable spin-lock sequence (ramp CPMAS) and a contact time of 1 ms, optimised into a range between 1 and 5 ms [16].

2.3.5. Liquid-state 2D NMR analysis

The citrus pectin (CP) and cross-linked citrus pectin (CLCP) were analysed through 2D NMR analysis to study its structural conformations. ^{1}H (500 MHz) and ^{13}C NMR (125 MHz) spectra were recorded on a Bruker BioSpin FT-NMR AvanceTM I 600 spectrometer for 3–5 %

solutions of polysaccharides in D_2O (99.9 % D) at 303 K (all spectra) and 328 K (selected 2D spectra). Two-dimensional homonuclear (COSY) and heteronuclear (HSQC and HMBC) spectra were recorded using standard Bruker procedures.

2.3.6. Size exclusion chromatography (SEC)

The molecular weight of samples was determined through a 515 Waters HPLC system coupled with Shodex OHpak LB-806 M column for pectin. The differential refractive index data was collected through the Wyatt Optilab T-rEX detector, and the multi-angle light scattering data was collected through the Wyatt Down Heleos detector. The mobile phase was 50 mM $NaNO_3$ with a 0.5 mL/min flow rate. The samples were lyophilised and dissolved at a 1.5 mg/mL concentration in the mobile phase. Complete dissolution was achieved by stirring the solutions in a 2 mL Eppendorf overnight and at room temperature using a magnetic bar. Before injection, the sample solutions were filtered (Millipore Millex-GV PVDF 0.22 μm). The injection volume was 100 μL [5,17].

2.4. Packaging film development from modified citrus pectin

3 g of modified citrus pectin is dissolved in 100 mL of distilled water in a magnetic stirrer operating at 600 rpm and 50 °C for 20 min. 2 mL of glycerol was added to the resulting solution and mixed in a magnetic stirrer for 10 min, until complete homogenisation. The resultant filmogenic solution was poured into a Petri dish of 15 cm diameter. Then, the plates are dried in a hot air oven operating at 60 °C for 10 h until complete evaporation of water. The dried MCP films were peeled off from the plates and stored in a desiccator at ambient temperature for characterisation.

2.5. Characterisation of MCP packaging films

2.5.1. UV blocking, transparency and colour properties

The packaging films' UV blocking, Transparency, and Colour were assessed using a high-performance UV–Vis spectrophotometer (Lambda 650, PerkinElmer, Waltham, MA, USA) following the method described by [18]. The transparency of the films was measured by placing a rectangular film (1 × 3 cm) in a spectrophotometer cell and recording the film's light transmittance at 600 nm. The following equation calculated transparency:

$$\text{Transparency} = \frac{\log \%T}{b} \tag{1}$$

Where %T was the light transmittance at 600 nm, and b was the thickness of the film (mm).

The UV transmission spectra of films were analysed in the wavelength range between 200 and 400 nm. The UV protection percentage of the films for UVA (315–400 nm) and UVB (280–315 nm) were calculated using the following formulae.

$$\textit{UVA blocking}\ (\%) = 100 - \frac{\int_{315}^{400} T(\lambda)d(\lambda)}{\int_{315}^{400} d(\lambda)} \times 100 \tag{2}$$

$$\textit{UVB blocking}\ (\%) = 100 - \frac{\int_{280}^{315} T(\lambda)d(\lambda)}{\int_{280}^{315} d(\lambda)} \times 100 \tag{3}$$

The colour parameter tests were performed in the wavelength range of (400–800 nm) operating at transmission mode. CIE L* (lightness), a* (redness) and b* (yellowness) values were obtained using visible region illuminant (light source). The area view and port size (diameter) were 0.64 cm^2 and 1.02 cm, respectively, and the observer angle was 10°. The following equation used the gathered colour parameters to calculate overall colour change (ΔE) in CLCP packaging films compared to ideal transparent film. Where, L_0–50, a_0–0, b_0–0 for the ideal transparent film (origin of the colour scale).

$$\Delta E = \sqrt{\left(L^* - L_0^*\right)^2 + \left(a^* - a_0^*\right)^2 + \left(b^* - b_0^*\right)^2} \tag{4}$$

2.5.2. Mechanical properties

Mechanical properties of the CLCP films were assessed using a dynamometer (model Z005, Zwick Roell, Ulm, Germany) and the software TestXpert V10.11 for data analysis. The elastic modulus (E_T, in MPa), the elongation at break (ε_B, in %), and the tensile strength (TS, in MPa) were determined on film strips 15 cm in length and 2.54 cm in width, according to ASTM D882. Tests employed a 5-kN load cell connected with two clamps 10 cm apart [19].

2.5.3. Oxygen and water vapour barrier properties

All polymeric films' oxygen and water vapour barrier properties were investigated on a 50 cm^2 surface sample using a TotalPerm permeability analyser (ExtraSolution®Srl, Capannori, Italy) based on the isostatic method and equipped with a double sensor system, that is, an electrochemical sensor for oxygen and an infrared sensor for water vapour. The oxygen transmission rate (OTR, in $cm^3\ m^{-2}\ day^{-1}$) was determined at 23 °C and 50 % relative humidity (RH), according to the standard methods ASTM F2476 and ASTM F2622, respectively, with a carrier flow (N_2) of 10 mL min^{-1} and a one-atmosphere analyte partial pressure difference between the specimen's two sides. For OTR, values at a 0.21 partial pressure difference were also calculated to simulate the oxygen barrier performance under natural (atmospheric) conditions. The water vapour transmission rate (WVTR, in g $m^{-2}\ day^{-1}$) was measured according to the ASTM F1249 standard method, with a carrier flow (N_2) of 10 mL min^{-1} at 38 °C and 90 % RH (tropical conditions). All the analyses were conducted with each sample's external side (i.e., the external environment) facing the upper semi-chamber, where the humid test gas (i.e., oxygen) was flushed [19].

2.5.4. Surface morphology

The in-depth surface morphology of the films was determined using a ToscaTM 400 AFM (Anton Paar Italia Srl, Rivoli, Italy) in contact resonance amplitude imaging (CRAI) mode. Towards this goal, an Arrow-FMR-10 Force Modulation probe (Nanoworld, Neuchâtel, Switzerland) featuring a rectangular cantilever with a triangular free end and a tetrahedral tip with a typical height of 10–15 μm was used. Additionally, the tip radius of curvature is ~10 nm. The cantilever has a spring constant and resonance frequency of 2.8 N m^{-1} and 75 kHz, respectively. For the analyses, approximately 1 × 3 cm film sample was placed onto a mica disc substrate (Ted Pella Inc., Redding, California). Dimensional calculations and image editing were conducted via Digital Surf Mountains Analysis Software [16]. The mean root mean square surface roughness values reported for each film dimension were calculated using at least five images.

2.5.5. Water contact angle

The water contact angle of the film surfaces was assessed using an optical contact angle apparatus (KSV CAM 200, Espoo, Finland) equipped with a Basler A602f camera. The contact angle of water in the air was measured on rectangular (5 × 2 cm^2) film samples by the sessile drop method. This method gently drops a 4 ± 0.5 μL droplet of Milli-Q water (18.3 MΩ cm) onto the coated surface. Specifically, a droplet hanging on the end of a needle is laid on the film surface by raising the sample stage until solid/liquid contact is made. Analyses were conducted in a climate-controlled room (23 °C and 50 % relative humidity (RH)). All droplets were released from a height of 1 cm above the surface to ensure consistency between each measurement. The evolution of the contact angle (θ, the angle between the baseline of the drop and the tangent at the drop boundary), the droplet volume (V, μL) and the droplet surface area (A, mm^2) were monitored using a software-assisted

Table 1
Central Composite trail design for the bulk modification of citrus pectin with stearic acid.

Trails	pH	Temperature [°C]	Time [h]	Modification percentage [%]
1	6	40	24	17.11 ± 1.37
2	8	50	24	17.85 ± 1.53
3	6	60	24	18.94 ± 1.66
4	7	40	24	22.29 ± 1.28
5	7	60	24	25.78 ± 1.79
6	8	40	24	17.38 ± 1.42
7	8	60	24	20.24 ± 1.44
8	6	40	48	23.54 ± 1.62
9	6	50	48	24.71 ± 1.57
10	6	60	48	27.68 ± 1.74
11	7	40	48	33.27 ± 1.98
12	7	50	48	36.54 ± 1.47
13	8	40	48	24.13 ± 1.35
14	8	50	48	25.34 ± 1.85
15	6	50	72	27.63 ± 1.31
16	6	60	72	29.79 ± 1.65
17	7	40	72	35.11 ± 1.33
18	7	50	72	39.54 ± 1.58
19	7	60	72	43.35 ± 1.81
20	8	50	72	30.54 ± 1.43

Modification percentage is a relative value calculated from the FTIR peak area ratio of A ~ 1735 cm^{-1} / A ~ 1104 cm^{-1}.

image processing procedure, which fits the drop profile with the Young-Laplace equation. The values of these parameters were collected 2 times per second during the first 10 s and 1 time per second during the following 50 s of analysis, starting from the drop deposition.

2.6. Statistical Analysis

All analyses for each treatment group were conducted in five independent repetitions, and the average value for each analysis was evaluated from the repetitions. The results are represented in the form of mean ± standard error. Face-centred central composite design (FC-CCD) experiments were developed to investigate the stearic acid modification of citrus pectin. The reaction parameters for the central composite design were selected based on preliminary studies. The temperature range of 40–60 °C was chosen to ensure sufficient reaction kinetics without causing thermal denaturation of the enzyme. The pH range of 6–8 was selected as lipase often exhibits a broad activity profile around neutral pH in bi-phasic systems, avoiding extreme conditions that could lead to pectin degradation via hydrolysis or β-elimination. Reaction times of 24–72 h were investigated to allow the heterogeneous reaction to proceed towards completion. These CCD data were analysed through the principal component analysis (PCA) framework (Analyse-it Software, Leeds, UK) to evaluate the influence and correlation of different conditions on the output modification percentage of pectin. The film

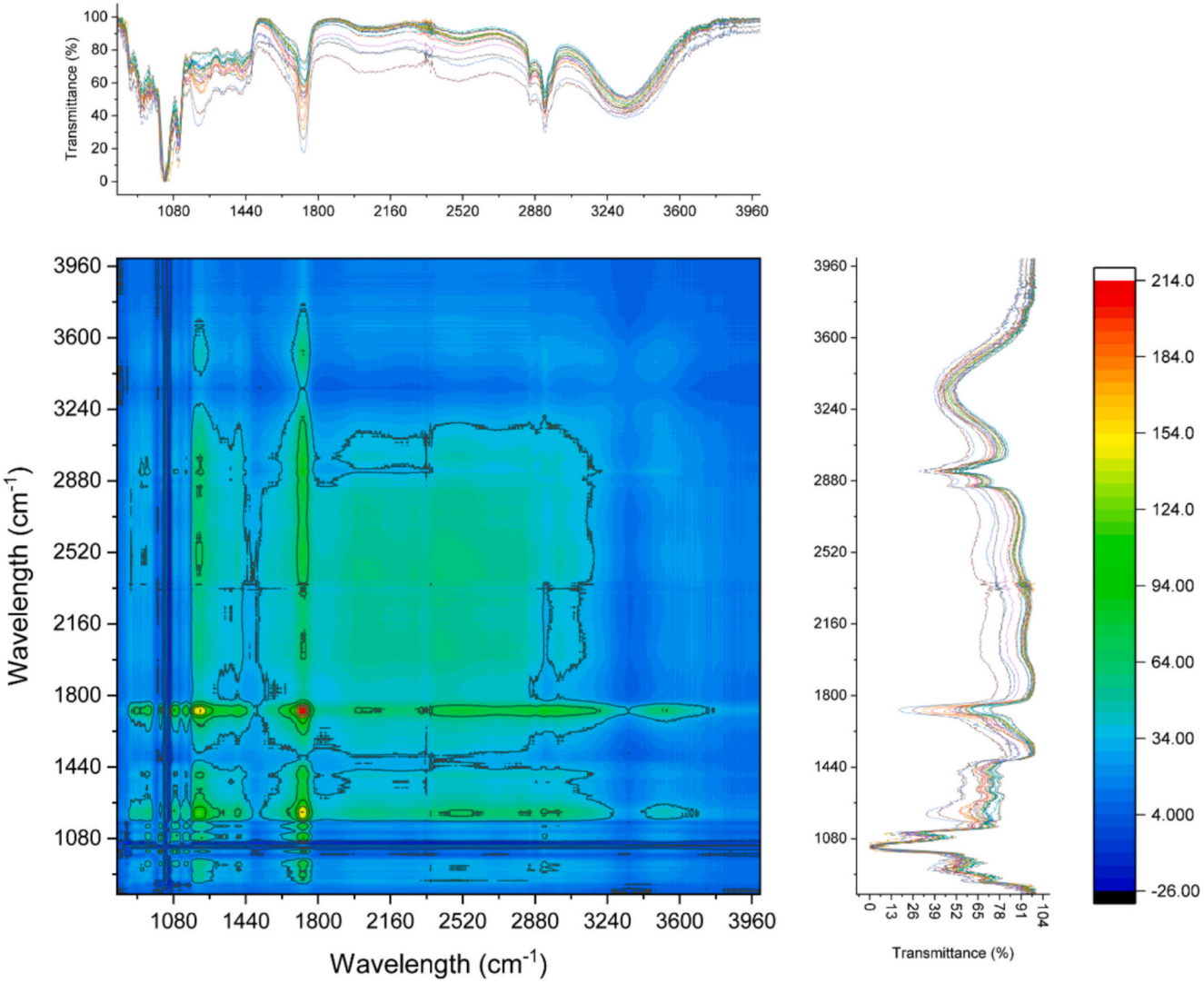

Fig. 1. 2D FTIR homo correlation spectra of MCP production trials.

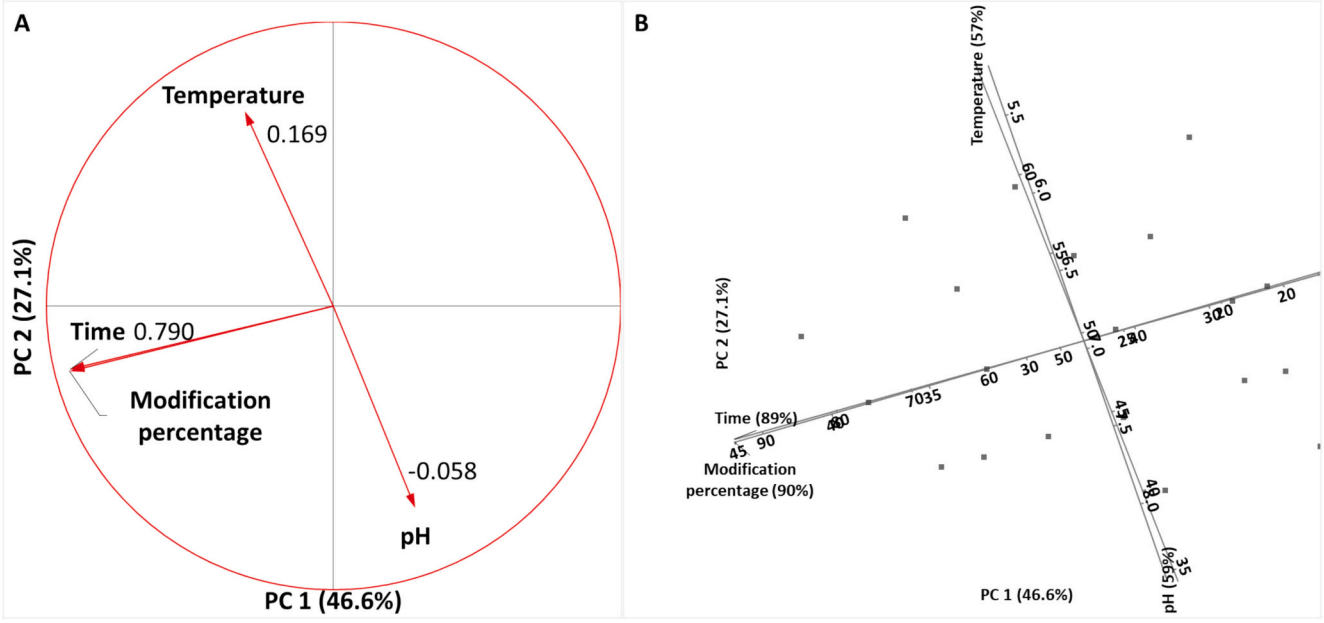

Fig. 2. Principal component analysis for modification of citrus pectin with stearic acid [A – Monoplot; B – Biplot].

characteristic data were analysed using a one-way analysis of variance to check for differences between samples. The significance level (*P*) was fixed at 0.05.

3. Results and discussions

3.1. Modification of citrus pectin with stearic acid in bi-phasic reaction

The pectin molecules extracted from citrus industrial wastes were subjected to enzymatic modification with stearic acid in a bi-phasic reaction system. The central composite design of experiments (Table 1) was constructed to observe the effects of pH, reaction temperature, and reaction time. The reacted pectin samples were analysed with FTIR, and the infrared spectra of all the trails were subjected to 2D symmetric correlation analysis. The 2D symmetric FTIR correlation spectra (Fig. 1) revealed that there is a significant change in spectra around ~1700 cm^{-1}, corresponding to the increase in COOR ester group formation with stearic acid. [12] worked on the enzymatic grafting of resorcinol with pectin and observed that the grafting could be confirmed with a change in FTIR absorption peak around 1734 cm^{-1}. Similar observations were made by [11] on enzymatic amidation of pectin. The pectin modification CCD data was subjected to principal component analysis to analyse the effect of each parameter on pectin modification. The Mono and Bi-plot of principal component analysis data with correlation vectors are

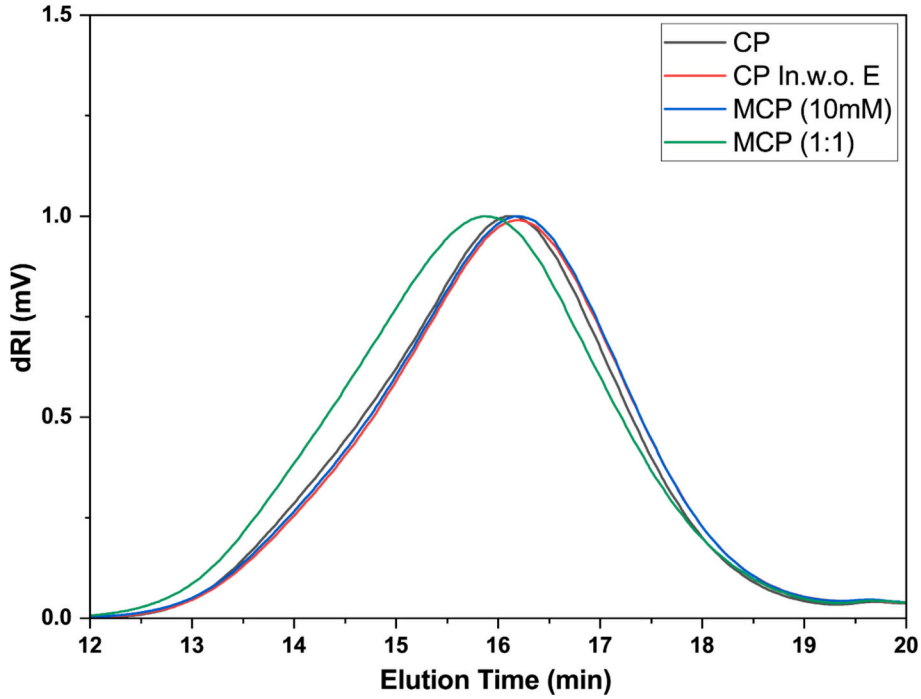

Fig. 3. Molecular weight distribution of modified citrus pectin at different reaction conditions.

Table 2
Average molecular mass distribution and polydispersity index of stearic acid grafted modified citrus pectin.

Sample	Mn	Mw	Mz	Polydispersity
Units	kDa	kDa	kDa	Mw/Mn
CP	78.12	**167.1**	1423.4	2.139
CP Incubated without enzyme (Control)	75.17	**166.9**	468.2	2.221
CP reacted with 10 mM Stearic acid	77.57	**171.3**	483.7	2.208
CP reacted with stearic acid in the Molar ratio (1:1)	108.9	**221.2**	538.8	2.031

Where Mn – Number Average Molar Mass; Mw – Weight Average Molar Mass; Mz – z Average Molar Mass.

illustrated in Fig. 2. The pectin modification percentage was observed to have a high positive correlation with reaction time and a moderate positive correlation with reaction temperature. The selected pH range for the reaction had almost nil effect on the modification percentage. This may be attributed to the fact that lipase has a wide pH range for its activity in bi-phasic reaction conditions [20]. The overall reaction data analysis implies that the enzymatic modification of citrus pectin with stearic acid highly depends on the reaction temperature and time. The maximum modification percentage of 43.35 ± 1.81 % was achieved in the pH of 7, with reaction temperature and time of 60 °C and 72 h, respectively.

3.2. Physical characteristics of modified citrus pectin

The molecular weight of pectin is a crucial factor in the formation and properties of pectin-based packaging films. High molecular weight pectin generally leads to more robust and more cohesive films due to the increased chain entanglement and intermolecular interactions, which enhance mechanical properties like tensile strength and elasticity [21,22]. Additionally, films made from high molecular weight pectin tend to have better barrier properties, offering improved moisture and gas transmission resistance. Conversely, lower molecular weight pectin can result in more brittle films and less effective barriers [23]. Therefore, controlling the molecular weight of pectin is essential for optimising the performance and functionality of packaging films to meet specific application requirements. The molecular weight distribution pattern of citrus pectin and stearic acid grafted modified citrus pectin are illustrated in Fig. 3. The molecular weight calculations with polydispersity index of modified citrus pectin are tabulated in Table 2. Three different molecular weights can be calculated for polymers: number average molar mass, weight average molar mass, and zeta average molar mass. Among the parameters mentioned above, weight average molar mass is considered for natural polymers since they have a high polydispersity index. The average molecular weight of CP was estimated to be 167.1 kDa. The average molecular weight of CP reacted with a 10 mM concentration of stearic acid was estimated at 171.3 kDa. This increase in molecular weight was not significant enough to affect the water vapour transmission resistance and water contact angle of the modified pectin packaging films. Thus, the reaction was enhanced with a 1:1 M ratio between CP and stearic acid, significantly increasing the average molecular weight to 221.2 kDa. This represents a significant increase of 54.1 kDa, confirming the successful grafting of stearic acid onto the pectin backbone. **Polydispersity** is a value of the molecular weight dispersion in the polymer sample. The higher the value, the greater the polydispersity. A value of 1 indicates a monodisperse sample (i.e. a sample in which all molecules have the same molecular weight) [24]. [25], studied the effect of nanocellulose-reinforced pectin films on the shelf life of chicken meat and observed that low polydispersity of polymers helps achieve better mechanical properties. However, being a plant-based polymer, the pectin molecules were observed to have a polydispersity value of above 1 by many researchers [26,27] The polydispersity of all the investigated samples was above 2, indicating that the samples have pectin molecules of different molecular weights. The difference in molecular weight between CP and MCP is 54.1 kDa, indicating the grafting of ~190 molecules of stearic acid in 1 molecule of CP.

The particle size of pectin is a crucial factor influencing the formation and quality of pectin-based packaging films. Smaller pectin particles can produce a more uniform and smooth film, enhancing its mechanical properties and barrier performance against moisture and gases [28]. Fine particles ensure better dispersion and more consistent film formation, reducing the likelihood of defects such as pinholes or uneven thickness [29]. This uniformity is crucial for maintaining the film's structural integrity and functionality. Additionally, smaller particle sizes can improve the film's transparency and aesthetic appeal, making it more suitable for consumer packaging. Thus, investigating the particle size of pectin is essential for producing high-quality, effective packaging films. The particle size distribution of the CP and MCP are illustrated in Fig. 4A. The average particle size of CP and MCP was estimated to be 889 nm and 1184 nm, respectively. This increase in particle size, in collaboration with molecular weight, can be ascribed to the effective grafting of stearic acid molecules in CP. **The zeta potential** of pectin is a critical parameter in the formation and stability of pectin-based packaging films. Zeta potential indicates the surface charge of

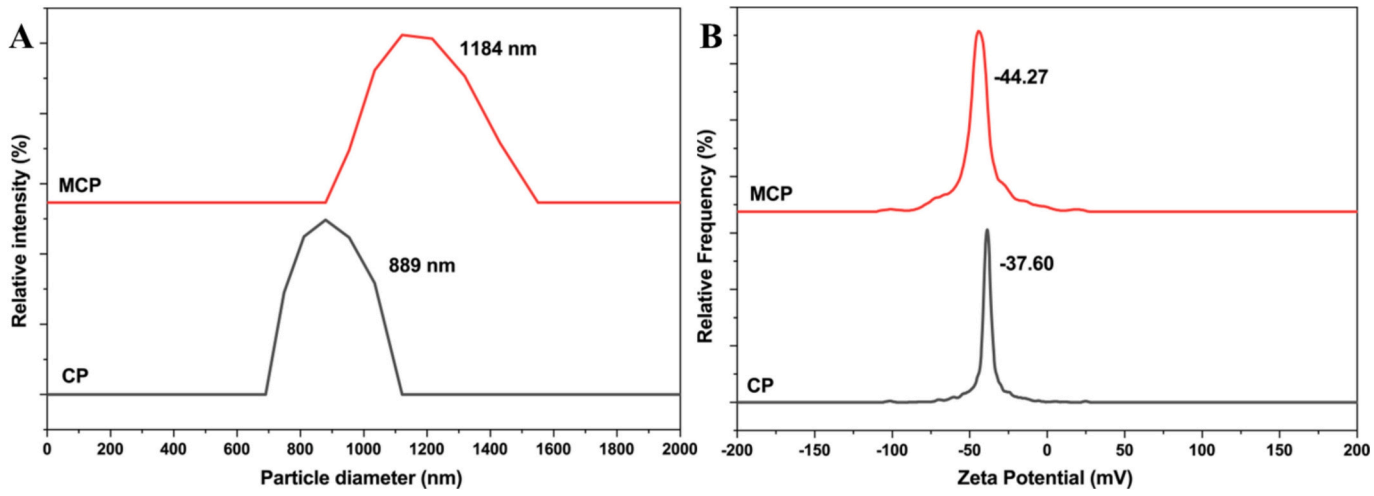

Fig. 4. Particle size distribution (A) and zeta potential (B) of unmodified citrus pectin (CP) and modified citrus pectin (MCP) prepared under optimal conditions (pH 7, 60 °C, 72 h).

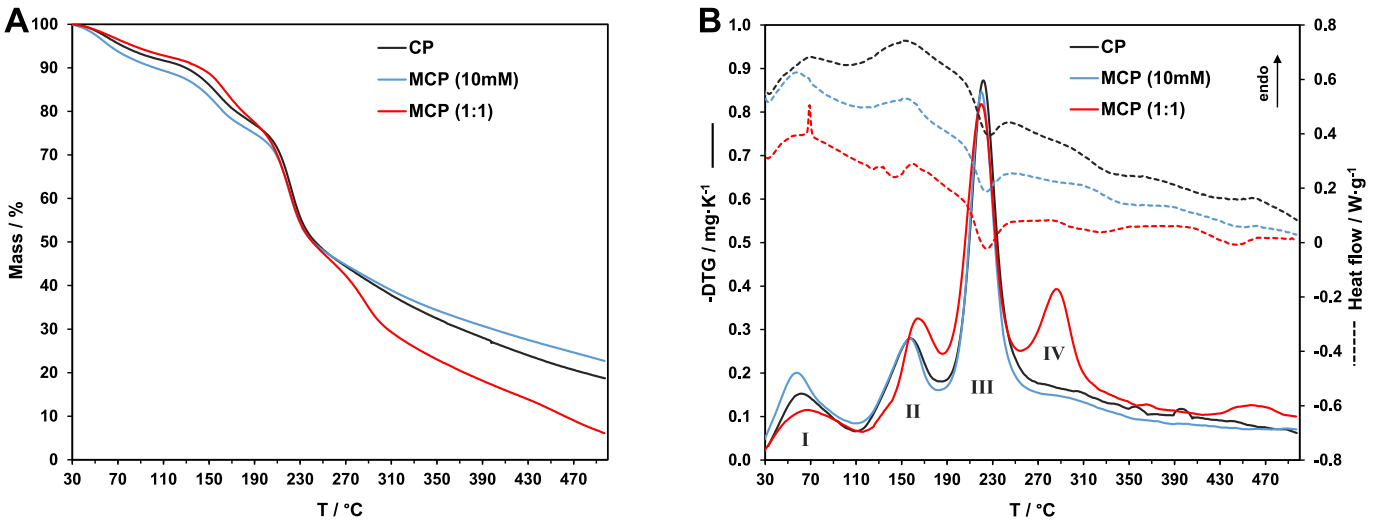

Fig. 5. Thermal degradation analysis of CP and MCP at different reaction conditions [A – Thermogravimetric profiles; B – DTG and DSC thermograms].

pectin particles in suspension, influencing their dispersion, aggregation, and overall stability during film formation [24]. A high absolute zeta potential value, positive or negative, typically signifies good electrostatic repulsion between particles, preventing aggregation and leading to a more uniform and homogenous film. This uniformity is essential for achieving desirable mechanical properties, such as tensile strength and flexibility, and enhancing the film's barrier properties against moisture and gases [30]. Therefore, investigation of the zeta potential of pectin ensures the production of stable, high-quality packaging films with consistent performance and reliability. The zeta potential of CP and MCP was estimated to be −37.60 mV and − 44.27 mV, respectively. This increase in zeta potential can be attributed to the attachment of stearic acid molecules in the backbone of CP, affecting each CP molecule's overall charge. This also facilitates the uniform distribution of MCP molecules in MCP filmogenic solution, resulting in the formation of a homogeneous film without micropores, which can affect the functional properties of the packaging films.

The thermal degradation properties of the modified citrus pectin, with SA:CP molar ratios of 1:1 and 0.01:1 (i.e., MCP 10 mM), are illustrated in Fig. 5 in comparison with the original citrus pectin (reported from the previous work (Chandrasekar, et al., 2024).

The TG traces reported in Fig. 5A show slightly different patterns of mass loss for CP (Chandrasekar, et al., 2024) and MCP at 1:1 SA:CP molar ratio that reveal a quite similar resistance against thermal degradation up to about 260 °C, whereas a further degradation event is exhibited by MCP. For the sake of comparison, MCP obtained as 0.01:1 SA:CP molar ratio followed the same pattern exhibited by the unmodified CP, indicating that the amount of SA was not enough to produce any visible modification in the pectin thermal stability against degradation. Indeed, beside the similarities in the thermogravimetric traces between CP and MCP (10 mM), the mass residues left by each at 500 °C are similar as well and correspond to about 19 % and 23 %, respectively, whereas a mass residue of about 6 % is left at 500 °C by MCP (1:1).

To better discriminate the phenomena lying under the mass loss across the temperature range considered, Fig. 5B reports the temperature derivative (DTG) of the three TG traces shown in panel A, as well as the thermal effects involved in the process.

As already described in the previous work (Chandrasekar, et al., 2024), the DTG trace for CP in Fig. 5B shows three main peaks corresponding to main mass loss events, which clearly involve thermal effects. Briefly, DTG peaks I and II are associated to two endothermic events that can be ascribed to diffusional and bound water loss, respectively; instead, peak III, with a maximum at about 222 °C, reflects the pyrolytic decomposition of the polysaccharide, as confirmed by the exothermic event recorded in the heat flow trace between 190 °C and 260 °C, leading to the evolution of several gaseous products (due to decarboxylation) and to the formation of solid char [31,32]. The latest part of the DTG trace (above 260 °C) shows a slower mass loss ascribable

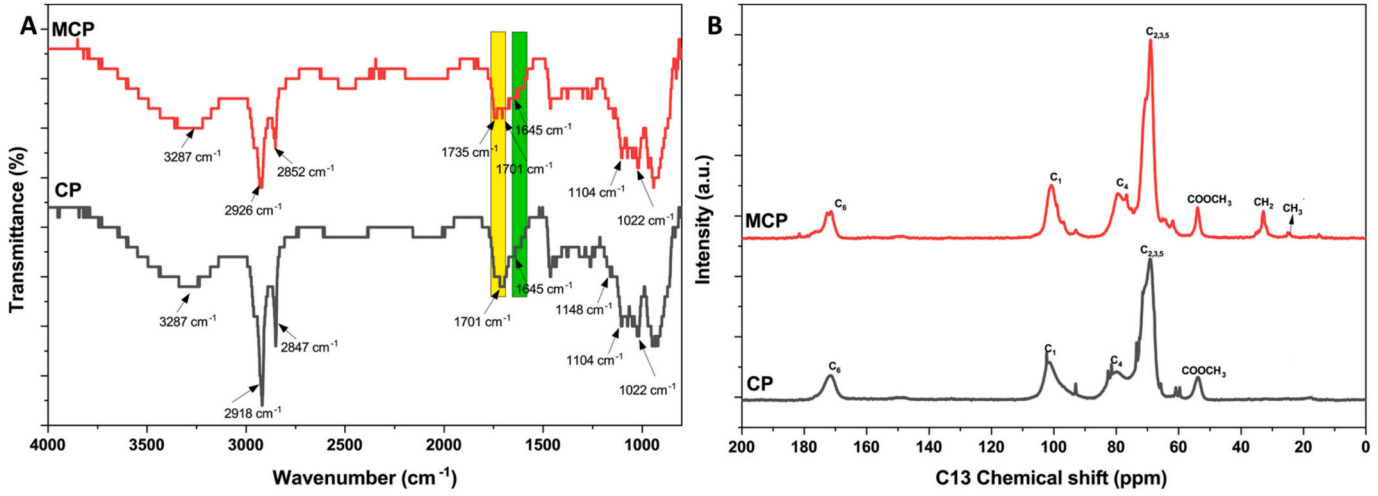

Fig. 6. FTIR spectra and CP-MAS NMR spectra of modified citrus pectin.

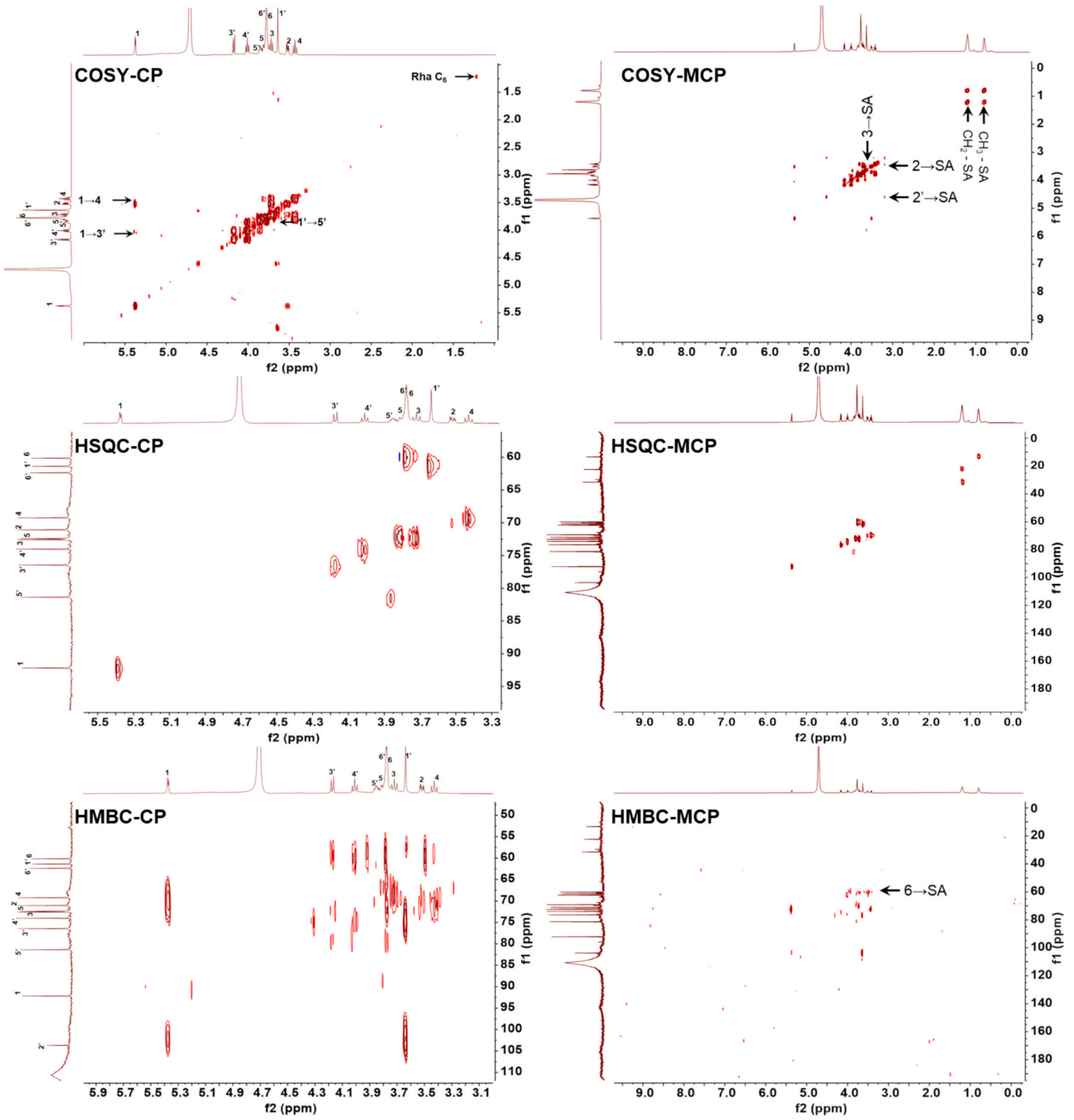

Fig. 7. 2D NMR spectra of CP and MCP [Important Note: Hexose monosaccharides noted in CP are galacturonic acid, galactose, fucose, rhamnose, glucose, and glucuronic acid. Pentose monosaccharides noted in CP are xylose and arabinose. Hexose monosaccharides' general structural form is of a pyranose ring where carbon and protons are indicated in the 2D NMR as 1, 2, 3….etc. Pentose monosaccharides' general structural form is of a furanose ring where carbon and protons are indicated in the 2D NMR as 1′, 2′, 3′…. etc.]

to further thermal degradation of the remaining char.

As concerns MCP (1:1), the DTG trace shown in Fig. 5B reveals only slight differences with respect to CP up to about 260 °C, as already anticipated by the mass loss profiles. More specifically, although the water loss-related peaks (I and II) are still present, we may observe a reduced intensity of peak I and a slight upshift of peak II towards higher temperatures: this evidence reveals a reduced ability of the matrix to adsorb atmospheric moisture upon modification (less free or diffusional water is released in peak I) as well as a greater energy required to remove the remaining bound water (upshift of peak II). Both of these indicators are consistent with the increased hydrophobicity of the MCP structure due to the grafted stearic acid chains [33,34]. Analogously, also the main degradation peak III seems to be only slightly affected by the matrix modification since such a degradation event appears to start earlier than the CP's. Similar behaviours have already been reported in the literature for differently modified pectin (through both esterification and acylation) [33–35] and might be ascribed to the degradation of the least ordered region of the matrix. On the other hand, a fourth peak in

Table 3
Chemical shift assignments for CP and MCP.

Assigned group and bond names	COSY		HSQC		HMBC	
	Chemical shift (ppm)					
	1H	1H	1H	13C	1H	13C
Citrus Pectin						
Pentose C1	3.64	3.64	3.64	61.51	3.64	61.51
Hexose C6	3.76, 3.78	3.76, 3.78	3.76, 3.78	60.06	3.76, 3.78	59.78, 62.11
Hexose C4	3.42	3.42	3.41	69.22	3.41	69.31
Hexose C2	3.54	3.54	3.52	70	3.52	70
Hexose C3	3.69	3.69	3.70, 3.69	72.34, 72.34	3.69	72.34
Hexose C5	3.81	3.81	3.83, 3.81	72.34, 72.34	3.81	72.23
Pentose C4	4.01	4.01	4.02, 4.01, 3.86	74.29, 73.90, 73.90	4.01	74.09
Pentose C3	4.17	4.17	4.17	76.64	4.17	76.64
Pentose C5	3.85	3.85	3.85	81.46	3.85	81.46
Hexose C1	5.39	5.39	5.39	92.27	5.39	92.27
Pentose C3 → C4	4.17	4.01	4.04	76.64	4.04	76.64
Hexose C2 → C3	3.54	3.71	3.73	70	3.73	70
Hexose C3 → C4	3.71	3.42	3.72	69.61	3.72	69.61
Hexose C3 → Pentose C1	3.7	3.64	3.71	61.35	nd	nd
Hexose C1 → Pentose C2	nd	nd	nd	nd	5.37	102.03
Hexose C1 → Hexose C4 (Gal/GalA linkages)	5.37	3.42	nd	nd	5.37	69.13
Pentose C1 → Pentose C5 (Arabinan Linkages)	3.63	3.85	nd	nd	3.83	61.48
Hexose C4 → Pentose C1	3.42	3.64	nd	nd	3.42	61.37
Hexose C2 → Pentose C1	3.53	3.64	nd	nd	3.51	61.22
Rhamnose C6	1.22	1.22	nd	nd	nd	nd
Stearic acid grafted modified pectin						
Observed Stearic acid characteristic Chemical shifts						
Terminal CH3 group	0.79	0.79	0.79	13.34	nd	nd
Intermediate CH2 groups	1.19	1.19	1.19	22.28	nd	nd
Terminal CH2 group adjacent to COOH	3.2	3.2	nd	nd	nd	nd
Observed linking of Stearic acid with Citrus Pectin						
Possible Linkage of terminal COOH with Hexose C2	3.2	3.54	3.2	69.8	nd	nd
Possible Linkage of terminal COOH with Pentose C2	3.2	4.59	nd	nd	nd	nd
Possible Linkage of terminal COOH with Hexose C6	nd	nd	nd	nd	3.2	60
Possible linkage of terminal COOH with Hexose C3	3.2	3.7	nd	nd	nd	nd

Important note: Hexose monosaccharides noted in CP are galacturonic acid, galactose, fucose, rhamnose, glucose, and glucuronic acid. Pentose monosaccharides noted in CP are xylose and arabinose. Hexose monosaccharides' general structural form is of a pyranose ring where carbon and protons are indicated in the 2D NMR as 1, 2, 3, and so on. Pentose monosaccharides' general structural form is of a furanose ring where carbon and protons are indicated in the 2D NMR as 1′, 2′, 3′, and so on. Abbreviations: nd – not detected.

the DTG trace is exhibited by MCP between 260 °C and 320 °C with a maximum at about 290 °C, also reflected by a slight endothermic contribution. This event is not easily attributable to a very specific process at a molecular level. Nonetheless, according to the degradation pattern reported in the literature for stearic acid [36], we may argue that peak IV might reflect the release of stearic acid molecules that were somehow linked or also adsorbed to the matrix. The following part of the DTG thermogram still shows the further thermal degradation of the remaining char.

3.3. Chemical and structural characteristics of modified citrus pectin

The chemical and structural characteristics of the CP and MCP were analysed through FTIR, CP-MAS solid-state NMR, and 2D liquid-state NMR analysis. The FTIR and CP-MAS NMR spectra of CP and MCP are illustrated in Fig. 6. Both CP and MCP showed characteristic peaks of O—H stretching (3287 cm^{-1}), C—H stretching (2918 cm^{-1}), C═O stretching (1645 cm^{-1}), C-O-C glycosidic stretching (~1100–1000 cm^{-1}), and sugar ring skeletal vibrations (1148, 1104, and 939 cm^{-1}). Other researchers observed and reported similar band assignments [37–39]. The peak at around 1104 cm^{-1}, unaffected by foreign groups, is often utilised as a reference peak for semi-quantitatively measuring the strength of other absorption peaks in the spectrum [12]. The additional absorption peak around 1735 cm^{-1} observed in MCP, attributing to the COOR ester group, facilitates the esterification of OH groups in pectin's structural monomers with the COOH group of stearic acid. The characteristic NMR chemical shifts of C^1 (101.57), $C^{2,3,5}$ (73.59–65.27), C^4 (80.30), C^6 (171.68), and, $COOCH_3$ (53.98) were observed for both CP and MCP. Similar chemical shift frequencies were noted for pectins extracted from sweet potatoes [40], *Adansonia digitata* [41] and *Punica granatum* [42,43]. The characteristic stearic acid CH_3 and CH_2 resonance peaks were observed in MCP. The additional resonance peaks were observed in the C^6 region of pectin, corresponding to the ester formation with stearic acid. Even though both FTIR and CP-MAS NMR confirm the grafting of stearic acid with CP, the structural confirmation of the CP modification cannot be clearly understood with a one-dimensional analysis of the MCP. Thus, more advanced 2D-NMR analyses, such as COSY, HSQC, and HMBC, were performed for both CP and MCP to confirm the structural modifications of CP. The two-dimensional NMR spectra of CP and MCP are illustrated in Fig. 7. The corresponding chemical shifts and bond assignments are tabulated in Table 3. The correlation 2D NMR spectra showed characteristic peaks of Pentose and Hexose stable furanose and pyranose structures, respectively [44,45]. The characteristic peaks of hexose (pyranose ring structure) are attributed to the major monosaccharide composition of Galacturonic acid and Galactose, as observed in the monosaccharide composition of CP. These peaks can also be attributed to the trace amounts of Fucose, Rhamnose, Glucose and Glucuronic acid due to the overlapping of the characteristic pyranose structure of hexose. The characteristic furanose structure of Pentose monosaccharides was also observed ascribing to CP's Xylose and Arabinose composition. The correlation of Hexose C1 – C4 was noted in both COSY and HMBC NMR. This can be ascribed to the (1 → 4) glycosidic linkages between the Galacturonic acid backbone in the HG portion of the CP and the Galactan structure in the RG-II portion of the CP. The correlation of Pentose C1-C5 was noted in COSY and HMBC NMR, attributing to the (1 → 5) glycosidic linkages in the CP's Arabinan side chain in the RG-II portion. The characteristic CH_3 and CH_2 resonances of stearic acid were noted in the MCP's COSY and HSQC NMR spectra. Apart from the characteristic resonances, four possible ester formation resonances between stearic acid and CP were observed in the 2D-NMR spectra of MCP. Among these, three possible linkage resonances were observed with C^2, C^3 and C^6 of Hexose monosaccharides in CP, and one possible linkage resonance was observed with C^2 of pentose monosaccharides in CP. The observed structure of the MCP is depicted in Fig. 8.

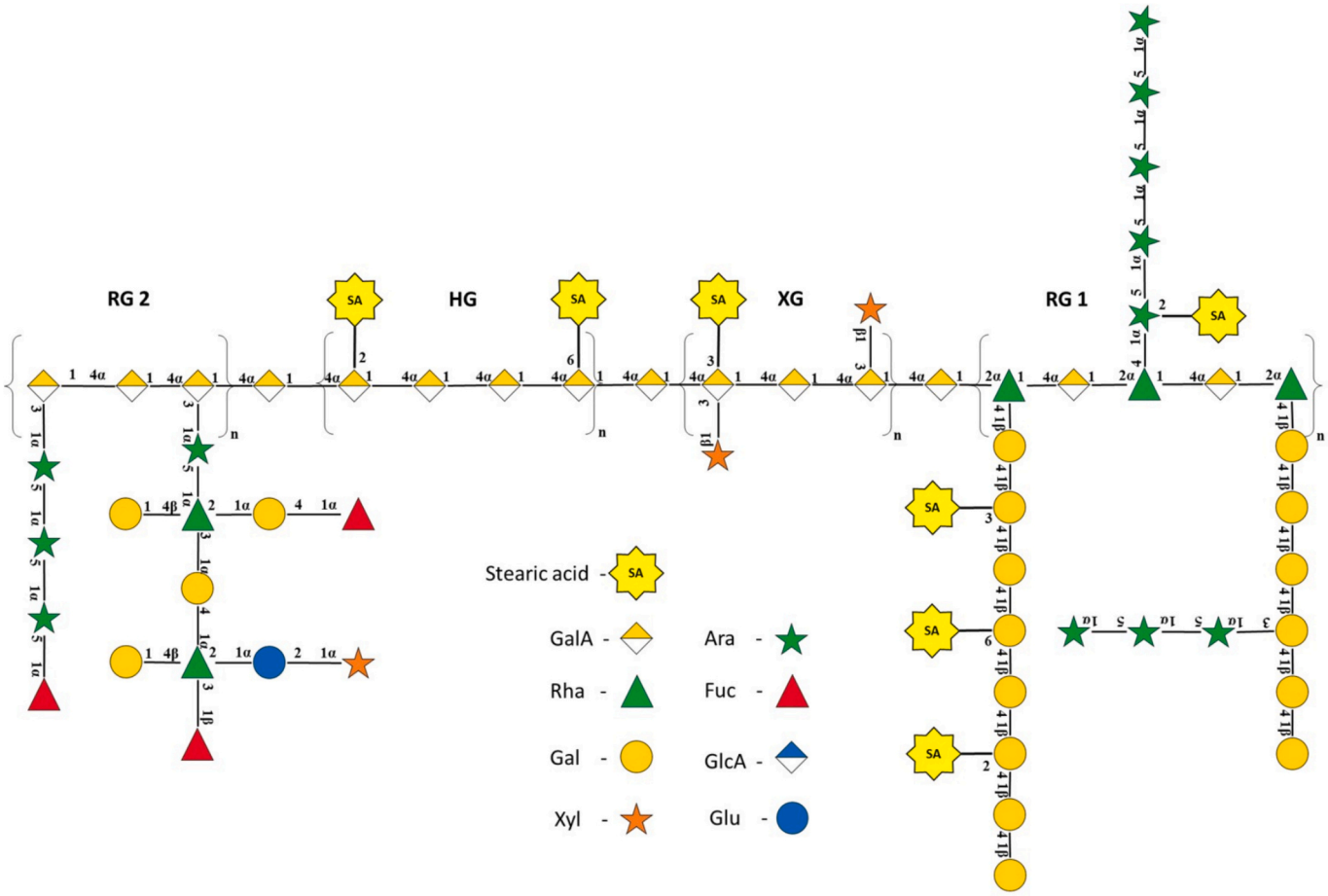

Fig. 8. The observed structure of modified citrus pectin (MCP). The basic structure of citrus pectin has been deduced from our initial characterisation work using Mass spec data of the enzyme-hydrolyzed fractions, and the 2D NMR has confirmed the modified structure of the citrus pectin. [Abbreviations:: HG - Homogalacturonan; RG – 1 - Rhamnogalacturonan-I; RG-2 - Rhamnogalacturonan-II; XG - Xylogalacturonan].

Table 4
Mechanical and barrier properties of the CP and MCP packaging films.

Samples	Average thickness	Tensile strength	Elongation at break	Elastic modulus	OTR @ 20 % RH	OTR @ 40 % RH	WVTR @ 40 % RH
	μm	MPa	%	MPa	$cm^3/(m^2.24h)$		$g/(m^2.24h.mmHg)$
CP film	114.20 ± 5.01	8.07 ± 2.45	16.74 ± 3.46	159.84 ± 36.24	0.23 ± 0.07 @ 21 % Oxygen 1.15 ± 0.04 @ 100 % Oxygen	1.34 ± 0.16 @ 21 % Oxygen 5.77 ± 1.14 @ 100 % Oxygen	26.34 ± 2.16
MCP film	119.83 ± 14.13	3.57 ± 0.56	5.66 ± 1.69	122.61 ± 18.61	0.19 ± 0.05 @ 21 % Oxygen 0.94 ± 0.04 @ 100 % Oxygen	0.96 ± 0.11 @ 21 % Oxygen 4.58 ± 1.14 @ 100 % Oxygen	17.80 ± 1.24

The values are given in Mean ± SE. Abbreviations: OTR – Oxygen transmission rate; RH – Relative humidity; WVTR – Water vapour transmission rate.

3.4. Development and characterisation of MCP-based packaging films

3.4.1. Characterisation of MCP films

The mechanical properties of pectin-based packaging films are critical for their functionality and durability in various applications. Properties such as tensile strength, elasticity, and elongation at break determine the film's ability to withstand handling, transportation, and storage without tearing or breaking [46]. Strong mechanical properties ensure that the films can protect their contents effectively, maintaining product integrity and safety. Additionally, good mechanical performance allows these films to be used in various packaging scenarios, from flexible pouches to rigid containers, enhancing their versatility [23]. Thus, optimising the mechanical properties of pectin-based films is essential for ensuring their reliability and effectiveness as packaging materials. The Mechanical and barrier properties of the CP and MCP packaging films are tabulated in Table 4. It was observed the MCP films have a significant ($P < 0.05$) reduction in all the mechanical properties compared to CP films. This reduction in the overall mechanical properties of the MCP films compared to the CP film can be attributed to the attachment of stearic acid in the free OH ends of the CP, which hinders the intra-molecular hydrogen bonding capabilities. Specifically, native pectin films derive their mechanical integrity from a dense, highly-ordered network of intermolecular hydrogen bonds. The successful grafting of bulky and hydrophobic stearic acid chains acts as a steric impediment, physically disrupting the close packing of the pectin backbones and preventing the re-formation of this cooperative network, leading to a less cohesive and more brittle material. The oxygen and water vapour barrier properties of pectin-based packaging films are crucial for preserving the quality and extending the shelf life of packaged goods. Effective oxygen barriers prevent oxidative spoilage,

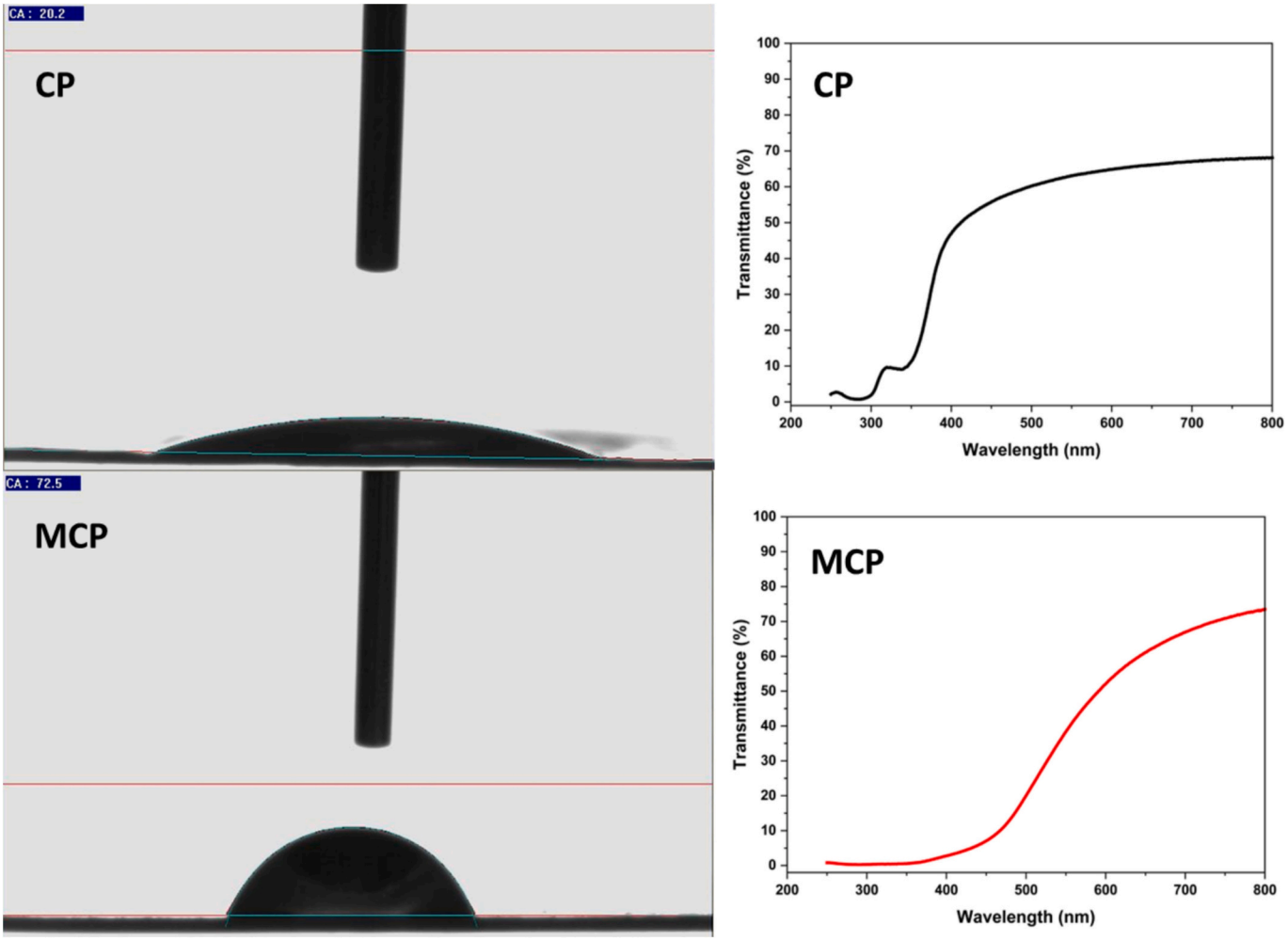

Fig. 9. Contact angle (Left) and UV-VIS Transmittance (Right) of CP and MCP packaging films.

leading to rancidity, discolouration, and nutrient degradation in food products [22,25]. Similarly, low water vapour permeability is essential to prevent moisture loss in dry products or moisture ingress in hygroscopic items, maintaining their texture, flavour, and freshness. The oxygen transmission rates of MCP films showed a significant ($P < 0.05$) reduction compared to CP films, both at 20 % and 40 % RH. Significant ($P < 0.05$) reductions in OTR were also noted between MCP and CP samples analysed at ambient 21 % oxygen and 100 % oxygen. The water vapour transmission rate of MCP films also showed a significant ($P < 0.05$) reduction compared to CP films. This improvement in barrier properties of MCP films can be attributed to the grafting of stearic acids to the monosaccharides of CP, which facilitates the water-repelling capacity of the films. The water-repelling capacity and UV-VIS transmission properties of the CP and MCP films were analysed through water contact angle and UV-VIS spectroscopic analysis (Fig. 9). The UVA (87.88 %) and UVB (98.93 %) blocking capacity of CP film was examined to be significantly ($P < 0.05$) lower than the UVA (99.42 %) and UVB (99.81 %) blocking capacity of the MCP films. However, the visible light transparency of the MCP films (4.81 mm^{-1}) was examined to be significantly lower than that of the CP films (5.44 mm^{-1}). This may be attributed to the modification of the pectin molecules by stearic acid. The colour change (ΔE) of the MCP films (13.09) was observed to be significantly higher than the CP films (9.06) from the ideal transparency parameters. The water contact angle of the MCP film (72.5°) showed a significant improvement ($P < 0.05$) of 52.3° compared to the CP film (20.2°). This proves the high surface water-repelling capacity of the MCP. This improvement in water-repelling capacity, in turn, results in the reduction of micropores in the film, resulting in the improvement of the oxygen barrier property of the MCP film. This phenomenon is evidently proved through the cross-sectional SEM analysis of the CP and MCP films. The cross-section of MCP films showed a tight arrangement of molecules, resulting in a smooth cross-section compared to CP films (Fig. 10). The surface morphology of the CP and MCP films was observed through SEM and AFM analysis. The AFM images were subjected to surface roughness measurement following the ISO 25178 method. The root mean square surface roughness of both CP (0.034 μm) and MCP (0.031 μm) films were found not to be significantly ($P > 0.05$) different from each other.

The thermal degradation properties of CP and MCP (1:1) films are compared in Fig. 11. The TG traces reported in Fig. 11A show slightly different patterns of mass loss for the films prepared from CP and MCP (1:1), that reflect a slightly different resistance against thermal degradation. Indeed, even considering the similarity in the mass residues left by each at 500 °C, correspond to about 11 % and 12 % for CP and MCP films, respectively. The main difference of about 10 % in terms of mass residue at about 250 °C (residue of about 23 % and 33 % for CP and MCP films, respectively) shows that higher temperatures are needed for MCP to complete the very late part of degradation.

To better highlight these phenomena, Fig. 11B reports the temperature derivative (DTG) of the two TG traces shown in panel A, as well as the thermal effects involved in the process.

As already described in Fig. 5 for powders, the DTG trace for CP film in Fig. 11B still shows three main peaks corresponding to main mass loss events. However, although DTG peaks I and II are again associated to

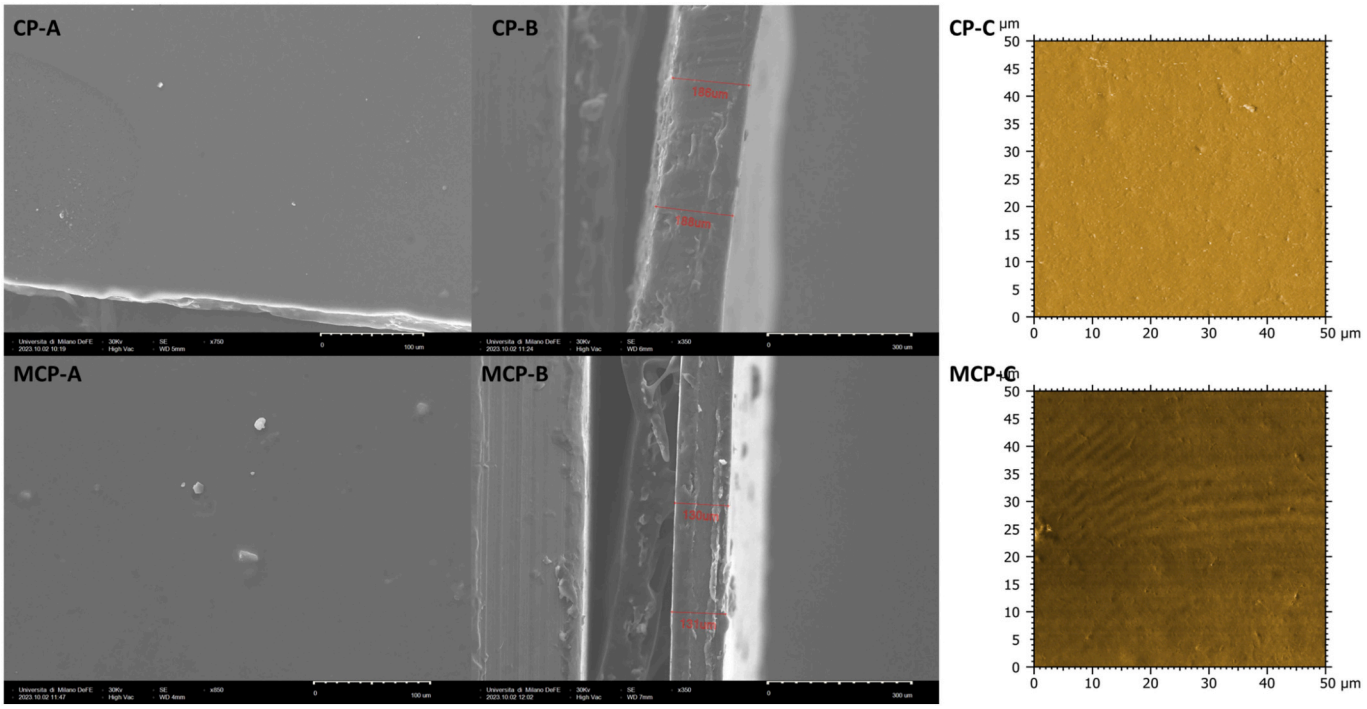

Fig. 10. Surface and cross-section morphology of CP and MCP packaging films [A – SEM surface image; B – SEM cross-section image; C – AFM surface image].

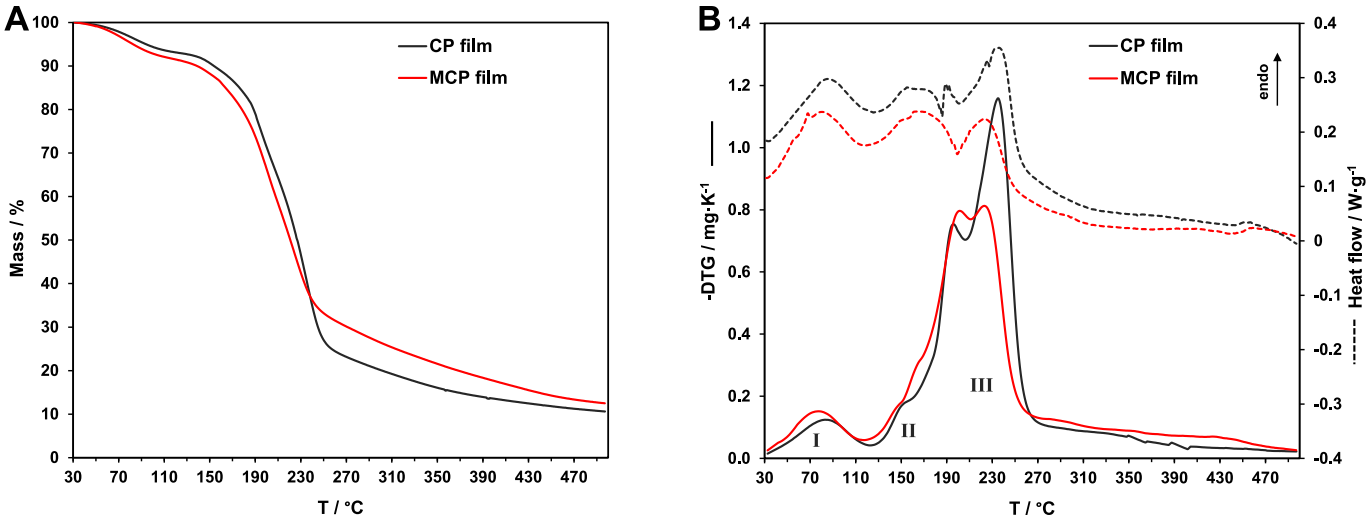

Fig. 11. Thermal degradation analysis of CP and MCP films [A – Thermogravimetric profiles; B – DTG and DSC thermograms].
Contextualizing Performance Trade-offs and Future Mitigation Strategies.

two endothermic events ascribable to diffusional and bound water loss, respectively, peak III becomes biphasic and appears to be associated to a heat flow trace (from about 180–270 °C) that clearly involves a superimposition of two main exothermic and endothermic events. The biphasic peak III firstly evidences the presence of CP region with different thermal stability. Furthermore, the presence of an endothermic event that does not occur in powders (Fig. 5B) suggests that the DTG trace within the same temperature region also involves a different process than the mere pectin degradation. Indeed, the 180–270 °C interval is compatible with the evaporation of the glycerol fraction used for the film preparation, which has been shown to occur within the same temperature interval interested by pectin degradation in our TGA-DSC direct measurements (Fiedot et al., 2024).

Concerning the MCP film, the DTG trace shown in Fig. 11B reflects the differences already visible from Fig. 11A. Although a biphasic peak III still occurs in the MCP's DTG profile, this peak covers a slightly reduced temperature interval (up to 260 °C). This evidence indicates that a certain percentage of the sample undergoes degradation below 260 °C, whereas a higher percentage of the thermal degradation process is completed between 260 and 500 °C than CP film. This is revealed by the higher intensity of the MCP's DTG trace when compared to the CP's. In any case, the 200–260 °C temperature interval is again associated with an abrupt endothermic event that likely reflects the evaporation of the glycerol fraction [47].

The observed inverse relationship between barrier and mechanical properties is a classic performance trade-off in polymer modification. This highlights that the developed MCP should be viewed not as a standalone product, but as a high-performance functional component

for advanced composite materials. Several strategies could mitigate this mechanical deficiency. One promising approach is developing nanocomposite films by incorporating reinforcing fillers like cellulose nanocrystals (CNC), which are known to significantly improve the mechanical properties of biopolymer films. Another effective strategy is polymer blending with a polymer capable of forming a strong network, such as starch, which can yield a synergistic composite with enhanced hardness and mechanical resistance.

4. Conclusion

The enzymatic modification of citrus pectin with stearic acid in a biphasic reaction system has demonstrated significant potential for improving the material properties of pectin-based packaging films. This study has shown that reaction time and temperature are critical factors influencing the degree of pectin modification, with optimal conditions identified at pH 7, 60 °C, and 72 h. The comprehensive chemical and structural analyses confirmed the successful grafting of stearic acid onto the pectin molecules, enhancing the material's functionality. The modifications increased molecular weight and particle size, which positively impacted the barrier properties of the films. Enhanced oxygen and water vapour barrier properties, along with improved UV-blocking and water-repelling capacities, indicate that modified citrus pectin (MCP) can effectively extend the shelf life and preserve the quality of packaged goods. These findings highlight the potential of MCP not as a standalone film, but as a specialized functional biopolymer for creating advanced composite and blended materials. Future work focused on integrating MCP with reinforcing agents like nanocellulose or structural polymers like starch is a promising avenue to develop fully functional, sustainable packaging solutions that leverage the enhanced barrier properties demonstrated in this study.

CRediT authorship contribution statement

Chandra Mohan Chandrasekar: Writing – review & editing, Writing – original draft, Validation, Supervision, Project administration, Methodology, Investigation, Formal analysis, Data curation, Conceptualization. **Daniele Carullo:** Formal analysis. **Francesca Saitta:** Formal analysis. **Tommaso Bellesia:** Formal analysis. **Enrico Caneva:** Formal analysis. **Carlo Baschieri:** Formal analysis. **Marco Signorelli:** Formal analysis. **Alberto Giuseppe Barbiroli:** Formal analysis. **Dimitrios Fessas:** Validation, Supervision. **Stefano Farris:** Validation, Supervision, Data curation. **Diego Romano:** Visualization, Validation, Supervision, Funding acquisition.

Declaration of competing interest

The authors declare that they have no known competing financial interests or personal relationships that could have appeared to influence the work reported in this paper.

Acknowledgements

The authors would like to acknowledge the financial support provided by Fondazione Cariplo (Project: CIRCLE, Citrus waste recycling for added-value products. 2020–1070) for the implementation of this project.

Data availability

No data was used for the research described in the article.

References

[1] S. Singhal, N.R. Swami Hulle, Citrus pectins: structural properties, extraction methods, modifications and applications in food systems – a review, Applied Food Research 2 (2022), https://doi.org/10.1016/j.afres.2022.100215.
[2] S.Q. Liew, N.L. Chin, Y.A. Yusof, K. Sowndhararajan, Comparison of Acidic and Enzymatic Pectin Extraction from Passion Fruit Peels and Its Gel Properties, J. Food Process Eng. 39 (2016) 501–511, https://doi.org/10.1111/jfpe.12243.
[3] H. Niu, X. Chen, X. Fu, B. Zhang, Z. Dou, Q. Huang, Pectin-stabilized emulsions: Structure-emulsification relationships, covalent and non-covalent modifications, and future trends, Trends Food Sci. Technol. 159 (2025), https://doi.org/10.1016/j.tifs.2025.104986.
[4] Z. Dou, Y. Tian, Y. Zhang, W. Zhang, Q. Duan, Q. Huang, B. Zhang, H. Niu, L. Wang, S. Zeng, Pectin-type polysaccharides from raspberry (Rubus idaeus L.): structure characterization and activity against DSS-induced colitis, Carbohydr. Polym. 364 (2025), https://doi.org/10.1016/j.carbpol.2025.123710.
[5] B. Neckebroeck, S.H.E. Verkempinck, J. Van Audenhove, T. Bernaerts, H. de Wilde d'Estmael, M.E. Hendrickx, A.M. Van Loey, Structural and emulsion stabilizing properties of pectin rich extracts obtained from different botanical sources, Food Res. Int. 141 (2021), https://doi.org/10.1016/j.foodres.2020.110087.
[6] J. Huang, Z. Hu, L. Hu, G. Li, Q. Yao, Y. Hu, Pectin-based active packaging: A critical review on preparation, physical properties and novel application in food preservation, Trends Food Sci. Technol. 118 (2021) 167–178, https://doi.org/10.1016/j.tifs.2021.09.026.
[7] S. Roy, R. Priyadarshi, L. Łopusiewicz, D. Biswas, V. Chandel, J.W. Rhim, Recent progress in pectin extraction, characterization, and pectin-based films for active food packaging applications: A review, Int. J. Biol. Macromol. 239 (2023), https://doi.org/10.1016/j.ijbiomac.2023.124248.
[8] H. Li, Y. Zhu, T.-X. Yang, Q.-S. Zhao, B. Zhao, Development and characterization of pectin-based composite film incorporated with cannabidiol/2,6-di-O-methyl-β-cyclodextrin inclusion complex for food packaging, Int. J. Biol. Macromol. (2024) 133525, https://doi.org/10.1016/j.ijbiomac.2024.133525.
[9] I.P. Butler, R.A. Banta, A.A. Tyuftin, J. Holmes, S. Pathania, J. Kerry, Pectin as a biopolymer source for packaging films using a circular economy approach: Origins, extraction, structure and films properties, Food Packag. Shelf Life 40 (2023), https://doi.org/10.1016/j.fpsl.2023.101224.
[10] S. Firdaus, F. Ahmad, S. Zaidi, Preparation and characterization of biodegradable food packaging films using lemon peel pectin and chitosan incorporated with neem leaf extract and its application on apricot fruit, Int. J. Biol. Macromol. 263 (2024), https://doi.org/10.1016/j.ijbiomac.2024.130358.
[11] C. Zheng, Y. Zou, Y. Huang, B. Shen, P. Fei, G. Zhang, Biosynthesis of amidated pectins with ultra-high viscosity and low gelation restriction through ultra-low temperature enzymatic method, Food Hydrocoll. 134 (2023), https://doi.org/10.1016/j.foodhyd.2022.108037.
[12] J. Liu, B. Chen, Q. Hu, Q. Zhang, B. Huang, P. Fei, Pectin grafted with resorcinol and 4-hexylresorcinol: Preparation, characterization and application in meat preservation, Int. J. Biol. Macromol. 237 (2023), https://doi.org/10.1016/j.ijbiomac.2023.124212.
[13] C.M. Chandrasekar, D. Carullo, F. Saitta, H. Krishnamachari, T. Bellesia, L. Nespoli, E. Caneva, C. Baschieri, M. Signorelli, A.G. Barbiroli, D. Fessas, S. Farris, D. Romano, Valorization of citrus peel industrial wastes for facile extraction of extractives, pectin, and cellulose nanocrystals through ultrasonication: An in-depth investigation, Carbohydr. Polym. 344 (2024), https://doi.org/10.1016/j.carbpol.2024.122539.
[14] C.M. Chandrasekar, L. Nespoli, T. Bellesia, M. Ghaani, S. Farris, D. Romano, Fabrication of double layer nanoparticle infused starch-based thermoplastic food packaging system for meat preservation, Int. J. Biol. Macromol. 254 (2024), https://doi.org/10.1016/j.ijbiomac.2023.127689.
[15] D. Zu-Man, Z. Yu-Long, T. Chun-Yang, L. Chuang, F. Jia-Qin, H. Qiang, C. Chun, Y. Li-Jun, T. Chin-Ping, N. Hui, F. Xiong, Construction of blackberry polysaccharide nano-selenium particles: Structure features and regulation effects of glucose/lipid metabolism in HepG2 cells, Food Res. Int. 187 (2024), https://doi.org/10.1016/j.foodres.2024.114428.
[16] C. Rovera, D. Carullo, T. Bellesia, D. Büyüktaş, M. Ghaani, E. Caneva, S. Farris, Extraction of high-quality grade cellulose and cellulose nanocrystals from different lignocellulosic agri-food wastes, Front Sustain Food Syst 6 (2023), https://doi.org/10.3389/fsufs.2022.1087867.
[17] L. Pitkänen, H. Sixta, Size-exclusion chromatography of cellulose: observations on the low-molar-mass fraction, Cellulose 27 (2020) 9217–9225, https://doi.org/10.1007/s10570-020-03419-9.
[18] C.M. Chandrasekar, H. Krishnamachari, S. Farris, D. Romano, Development and characterization of starch-based bioactive thermoplastic packaging films derived from banana peels, Carbohydrate Polymer Technologies and Applications 5 (2023), https://doi.org/10.1016/j.carpta.2023.100328.
[19] D. Carullo, A. Casson, C. Rovera, M. Ghaani, T. Bellesia, R. Guidetti, S. Farris, Testing a coated PE-based mono-material for food packaging applications: an in-depth performance comparison with conventional multi-layer configurations, Food Packag. Shelf Life 39 (2023), https://doi.org/10.1016/j.fpsl.2023.101143.
[20] V.D. Nimkande, S. Sivanesan, A. Bafana, Screening, identification, and characterization of lipase-producing halotolerant Bacillus altitudinis Ant19 from Antarctic soil, Arch. Microbiol. 205 (2023), https://doi.org/10.1007/s00203-023-03453-8.
[21] J. Yang, S. Punia Bangar, M. Rizwan Khan, G.A. Hammouda, P. Alam, W. Zhang, Biopolymer-based packaging films/edible coatings functionalized with ε-polylysine: New options for food preservation, Food Res. Int. 187 (2024), https://doi.org/10.1016/j.foodres.2024.114390.

[22] S. Mehraj, Y.S. Sistla, M. Garg, B. Santra, H.S. Grewal, A. Kanjilal, Improvement of moisture barrier and tensile properties of pectin films by incorporating *Terminalia catappa* Linn. leaf wax and xylitol, J. Polym. Environ. 31 (2023) 3522–3537, https://doi.org/10.1007/s10924-023-02805-1.
[23] V.G.L. Souza, I.P. Mello, O. Khalid, J.R.A. Pires, C. Rodrigues, M.M. Alves, C. Santos, A.L. Fernando, I. Coelhoso, Strategies to improve the barrier and mechanical properties of pectin films for food packaging: comparing nanocomposites with bilayers, Coatings 12 (2022), https://doi.org/10.3390/coatings12020108.
[24] M.V. Lorevice, G.S. Baccarin, J.R. Souza, P.I.C. Claro, M.R. de Moura, C.G. Otoni, L. H.C. Mattoso, Strengthening eco-friendly packaging from pectin by filling with poly(ε-caprolactone) nanoparticles and tailoring the degree of methyl-esterification, Mater Adv (2024), https://doi.org/10.1039/D4MA00033A.
[25] A. Tabatabaei, H. Ahari, S. Yousefi, B. Jannat, S.A. Anvar, Application of pectin/cellulose nanocrystal films loaded with summer savory essential oil as a novel packaging for chicken breast fillets, J. Food Meas. Charact. (2024), https://doi.org/10.1007/s11694-024-02557-z.
[26] Y. Jiang, C. Zhang, J. Yuan, Y. Wu, F. Li, D. Li, Q. Huang, Effects of pectin polydispersity on zein/pectin composite nanoparticles (ZAPs)as high internal-phase Pickering emulsion stabilizers, Carbohydr. Polym. 219 (2019) 77–86, https://doi.org/10.1016/j.carbpol.2019.05.025.
[27] Y. Zhao, D. Wang, P. Wang, W. Zhao, S. Zhao, Y. Ma, H. Chang, Y. Wang, Y. Liu, X. Zhao, Microbiota response of pectin determined by its structural characteristics during in vitro fecal fermentation: A comparative study of various pectin sources, Food Hydrocoll. 150 (2024), https://doi.org/10.1016/j.foodhyd.2024.109730.
[28] R. Villa-Rojas, A. Valdez-Fragoso, H. Mújica-Paz, Manufacturing Methods and Engineering Properties of Pectin-Based Nanobiocomposite Films, Food Eng. Rev. 10 (2018) 46–56, https://doi.org/10.1007/s12393-017-9163-9.
[29] F. Baghi, S. Ghnimi, G. Agusti, E. Dumas, A. Gharsallaoui, Development and characterization of pectin-based antimicrobial packaging films containing nanoemulsified Trans-cinnamaldehyde, Appl. Sci. (Switzerland) 14 (2024), https://doi.org/10.3390/app14062256.
[30] X. Fu, X. Chang, Z. Ding, H. Xu, H. Kong, F. Chen, R. Wang, Y. Shan, S. Ding, Fabrication and Characterization of Eco-Friendly Polyelectrolyte Bilayer Films Based on Chitosan and Different Types of Edible Citrus Pectin, Foods 11 (2022), https://doi.org/10.3390/foods11213536.
[31] W. Wang, X. Ma, P. Jiang, L. Hu, Z. Zhi, J. Chen, T. Ding, X. Ye, D. Liu, Characterization of pectin from grapefruit peel: A comparison of ultrasound-assisted and conventional heating extractions, Food Hydrocoll. 61 (2016), https://doi.org/10.1016/j.foodhyd.2016.06.019.
[32] U. Einhorn-Stoll, H. Kunzek, G. Dongowski, Thermal analysis of chemically and mechanically modified pectins, Food Hydrocoll. 21 (2007), https://doi.org/10.1016/j.foodhyd.2006.08.004.
[33] L. Monfregola, V. Bugatti, P. Amodeo, S. De Luca, V. Vittoria, Physical and water sorption properties of chemically modified pectin with an environmentally friendly process, Biomacromolecules 12 (2011), https://doi.org/10.1021/bm200376c.
[34] S. Seslija, P. Spasojević, V. Panić, M. Dobrzyńska-Mizera, B. Immirzi, J. Stevanović, I. Popović, Physico-chemical evaluation of hydrophobically modified pectin derivatives: Step toward application, Int. J. Biol. Macromol. 113 (2018), https://doi.org/10.1016/j.ijbiomac.2018.03.006.
[35] E.A.M.S. Almeida, S.P. Facchi, A.F. Martins, S. Nocchi, I.T.A. Schuquel, C. V. Nakamura, A.F. Rubira, E.C. Muniz, Synthesis and characterization of pectin derivative with antitumor property against Caco-2 colon cancer cells, Carbohydr. Polym. 115 (2015), https://doi.org/10.1016/j.carbpol.2014.08.085.
[36] S. Lerdkanchanaporn, D. Dollimore, An investigation of the evaporation of stearic acid using a simultaneous TG-DTA unit, Thermochim. Acta 324 (1998), https://doi.org/10.1016/S0040-6031(98)00519-X.
[37] Y.G. Xia, R.J. Zhu, Y. Shen, J. Liang, H.X. Kuang, A high methyl ester pectin polysaccharide from the root bark of *Aralia elata*: structural identification and biological activity, Int. J. Biol. Macromol. 159 (2020) 1206–1217, https://doi.org/10.1016/j.ijbiomac.2020.05.117.
[38] J. Wang, Z. Liu, X. Li, G. Liu, J. Zhao, Elucidating structure of pectin in ramie fiber to customize enzyme cocktail for high-efficiency enzymatic degumming, Carbohydr. Polym. 314 (2023), https://doi.org/10.1016/j.carbpol.2023.120954.
[39] T. Qi, J. Ren, X. Li, Q. An, N. Zhang, X. Jia, S. Pan, G. Fan, Z. Zhang, K. Wu, Structural characteristics and gel properties of pectin from citrus physiological premature fruit drop, Carbohydr. Polym. 309 (2023), https://doi.org/10.1016/j.carbpol.2023.120682.
[40] S. Nurdjanah, J. Hook, J. Paton, J. Paterson, Galacturonic Acid Content and Degree of Esterification of Pectin from Sweet Potato Starch Residue Detected Using 13 C, CP/MAS Solid State NMR, 2013.
[41] O.A. Patova, A. Luanda, N.M. Paderin, S.V. Popov, J.J. Makangara, S.P. Kuznetsov, E.N. Kalmykova, Xylogalacturonan-enriched pectin from the fruit pulp of Adansonia digitata: Structural characterization and antidepressant-like effect, Carbohydr. Polym. 262 (2021), https://doi.org/10.1016/j.carbpol.2021.117946.
[42] E.G. Shakhmatov, P.V. Toukach, E.N. Makarova, Structural studies of the pectic polysaccharide from fruits of Punica granatum, Carbohydr. Polym. 235 (2020), https://doi.org/10.1016/j.carbpol.2020.115978.
[43] E.G. Shakhmatov, E.N. Makarova, V.A. Belyy, Structural studies of biologically active pectin-containing polysaccharides of pomegranate Punica granatum, Int. J. Biol. Macromol. 122 (2019) 29–36, https://doi.org/10.1016/j.ijbiomac.2018.10.146.
[44] E. Aldred, Carbohydrates, in: Pharmacology, 2009, pp. 63–72, https://doi.org/10.1016/B978-0-443-06898-0.00009-8.
[45] D. Walczak, A. Sikorski, D. Grzywacz, A. Nowacki, B. Liberek, Identification of the furanose ring conformations and the factors driving their adoption, Carbohydr. Res. 526 (2023) 108780, https://doi.org/10.1016/J.CARRES.2023.108780.
[46] J.F. Mendes, L.B. Norcino, A. Manrich, A.C.M. Pinheiro, J.E. Oliveira, L.H. C. Mattoso, Characterization of pectin films integrated with cocoa butter by continuous casting: physical, thermal and barrier properties, J. Polym. Environ. 28 (2020) 2905–2917, https://doi.org/10.1007/s10924-020-01829-1.
[47] M. Fiedot, O. Rac-Rumijowska, P. Suchorska-Woźniak, M. Czajkowski, K. Szustakiewicz, M. Safandowska, A. Różański, A. Zdunek, W. Stawiński, J. Cybińska, H. Teterycz, J.F. Kennedy, The smart apple-based foil: The role of pectin-glycerol-lipid interactions on thermoresponsive mechanism, Food Hydrocoll. 154 (2024), https://doi.org/10.1016/j.foodhyd.2024.110067.